Adsorption 11: 725–730, 2005

Synthesis and Adsorption Characteristics of Nanoporous Graphite-Derived Carbon-Silica Composites

ZHENG-MING WANG*
PRESTO, Japan Science and Technology Agency and Applied Interfacial Chemistry RG, Research Institute for Environmental Management Technology, National Institute of Advanced Industrial Science and Technology, 2217-14 Hayashi-cho, Takamatsu-shi, Kagawa 761-0395, Japan
zm-wang@aist.go.jp

MIKI YAMAGISHI
Applied Interfacial Chemistry RG, Research Institute for Environmental Management Technology, National Institute of Advanced Industrial Science and Technology, 2217-14 Hayashi-cho, Takamatsu-shi Kagawa 761-0395, Japan

YINGHAO CHU
PRESTO, Japan Science and Technology Agency and Department of Chemical Engineering, Sichuan University, Chengdu, China

TAKAHIRO HIROTSU
Applied Interfacial Chemistry RG, Research Institute for Environmental Management Technology, National Institute of Advanced Industrial Science and Technology, 2217-14 Hayashi-cho, Takamatsu-shi Kagawa 761-0395, Japan

HIROFUMI KANOH
Center for Frontier Electronics and Photonics, Chiba University, 1-33 Yayoi-cho, Inage-ku, Chiba 263-8522, Japan

Abstract. A novel nanoporous C/SiO_2 composite was synthesized using graphite precursor by a soft chemical method and its adsorption properties were characterized by nonane, water, and nitrogen adsorption. It was found that only one part of micropores can strongly confine nonane molecules, indicating a wide micropore size distribution. Water adsorption leads to disappearance of one part of micropores, possibly due to closing of pores by dissociative adsorption of water on defective sites. Fractal analysis of the original and the differential nitrogen adsorption isotherms indicate that micropores have a rougher surface and mesopore a flatter surface, suggesting that micropores are surrounded by silica particles and mesopores involve the flat carbon layers.

Keywords: nanoporous, C/SiO_2 composite, adsorption

*To whom correspondence should be addressed.

1. Introduction

Nanoporous materials having large internal surface areas and tailored pore geometries play an important role in the field of adsorption, separation, and heterogeneous catalysis (Barton et al., 1999). One of the synthesis approaches for nanoporous materials is the route from layered materials such as clays by pillaring and intercalation methods (Barrer, 1978; Yamanaka et al., 1978; Pinnavaia, 1983; Yanagisawa et al., 1990; Landi et al., 1991; Inagaki et al., 1993). Graphite is a layered material having the thinnest atomic layer of all the layered materials. A nanoporous material with thin graphitic layers has been expected from the aims of high efficiency adsorption and gas storage (Matranga et al., 1992; Dresselhaus and William, 1999). Porous nanocomposites of hydrophobic carbon layers and active metal oxides are required for high efficiency catalytic performance and specific adsorption under moisture atmosphere (Marsh, 1989; Radovic, 1997).

In spite of a possible advantage of easy control to obtain a material having large surface area and tailored pore shape and size, nanoporous materials using graphite as the precursor has not yet been made by taking advantage of a soft chemical method. We have reported that nanoporous carbon/silica composites can be synthesized by hydrolyzing organic silicon alkoxides in the expanded interlayer of the oxidized product of graphite (Wang et al., 2002, 2003). The obtained novel porous nanocomposite of carbon and silica has a very high surface area and presents a medium hydrophilicity between the typical activated carbon and hydrophilic silica particles. Here, the nanoporous carbon/silica composite was synthesized and their porosities were further examined by adsorption and pre-adsorption techniques, and fractal analysis by using nonane, water, and nitrogen as the probes.

2. Experimental

2.1. Material Synthesis

The graphite-derived nanoporous carbon/silica composite was synthesized by using an oxidized product of natural graphite as the precursor, whose method was detailed in the previous reports (Wang et al., 2003). Briefly speaking, commercial natural graphite was oxidized by Staudenmier's method (Staudenmaier, 1898) to give the graphite oxide (GO) product. The interlayer of GO was pre-expanded by intercalation of long chain surfactant (hexadecyltrimethylammonium bromide) by adding surfactant into alkali-dispersed GO colloidal solution. The interlayer-pre-expanded GO was treated in tetraethoxylsilane (TEOS) at 298 K for 7 days. The final carbon-silica composite denoted $GOC_{16}S$-823 was obtained by calcination under vacuum at 823 K.

2.2. Characterization and Adsorption

Samples were characterized by various physicochemical methods such as X-ray diffraction (XRD), Thermal gravimetry/differential thermal analysis (TG/DTA), field-emission scanning electron microscope (FE/SEM), etc.

The first run (1 st-) adsorption isotherms of nonane, H_2O, and nitrogen on the sample were measured at 77 K for nitrogen and at 298 K for the others by a commercial volumetric apparatus (Belsorp 18, Nippon Bell Co., Osaka) after re-evacuating the sample at 623 K for water adsorption and at 823 K for the others for at least 2 h. After the 1st-run nonane adsorption, the adsorbent was successively evacuated at RT and 393 K each for 10 h, and at 823 K for 2 h, which steps are denoted n-1, n-2, and n-3, respectively, and nitrogen adsorption isotherms were measured at 77 K after each step.

Following the 1 st-run-water adsorption, the 2 nd- and 3 rd-runs water adsorption were carried out after evacuating the adsorbent pre-adsorbed in the previous run at 298 K for more than 3 h. After the finishing of three runs water adsorption, the adsorbent was evacuated at RT and 393 K each for 3 h, and at 823 K for 2 h, which steps are denoted w-1, w-2, and w-3, respectively, and nitrogen adsorption at 77 K were measured after each step.

Following the nitrogen adsorption after step w-3, other two nonane adsorption experiments, denoted 2 nd-w- and 3 rd-w-runs adsorption, were carried out at 298 K after evacuating the pre-adsorbed adsorbent at 298 K for 3 h, after which the adsorbent was again evacuated at 298 K for 3 h, which step is denoted wn-1. The final nitrogen adsorption was measured at 77 K after step wn-1.

3. Results and Discussion

3.1. Water and Nonane Adsorption

The obtained $GOC_{16}S$-823 has a black color, whose FE/SEM photo clearly presents the compacted wrinkled carbon layers composing with particles. XRD

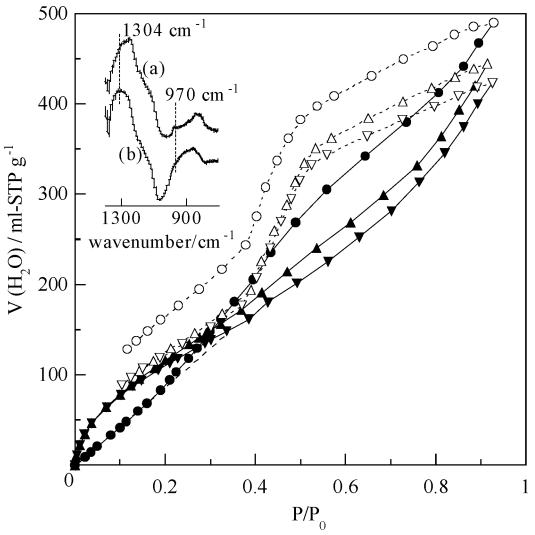

Figure 1. 1 st- (●, ○), 2 nd- (▲, △), and 3-rd (▼, ▽) runs H_2O adsorption isotherms at 298 K. The first and second symbols in the parenthesis represent the adsorption and desorption branches, respectively (the same in the following figures otherwise noted). The inset shows FT-IR spectra of $GOC_{16}S$-823 before (a) and after (b) H_2O adsorption measured at 393 K under continuous N_2 purge.

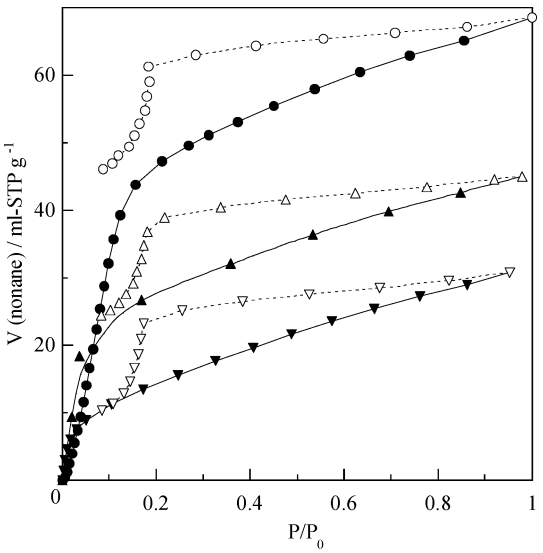

Figure 2. 1 st- (●, ○), 2 nd-w- (▲, △), and 3-rd-w- (▼, ▽) runs noane adsorption isotherms at 298 K.

measurement shows a disordered structure and the silicon content is 9.7 $\text{mmol} \cdot \text{g}^{-1}$ from TG/DTA measurement. Figure 1 shows the three runs water adsorption isotherms at 298 K. The 1 st-run-water adsorption isotherm presents a suppressed increase in adsorption at the low P/P_0 range, followed by a great uprising in adsorption from the medium P/P_0 range. Its desorption branch presents a great hysteresis at $P/P_0 = 0.4$ to 1, characteristic of mesoporosity, and an unclosed low-pressure hysteresis which indicates irreversible loss of the introduced H_2O molecules.

By the contrast, the adsorption isotherms of the 2 nd- and 3 rd-runs are of typical type IV shape (Gregg and Sing, 1982; Sing et al., 1985; Rouquerol et al., 1999) having a closed hysteresis branch. The greater uprisings in their adsorption amounts at the initial P/P_0 range indicate the improvement of surface hydrophilicity after the 1 st-run-adsorption. The almost overlapping amount of the two runs manifests the physical adsorptivity of water after the 1 st-run. However, lower adsorption of the two runs at higher P/P_0 range in comparison with that of the 1 st-run may suggest the loss of one part of porosity due to the 1 st-run-water adsorption.

Figure 2 shows the nonane adsorption isotherms of the 1 st-, 2 nd-w-, and 3 rd-w-runs at 298 K. The 1 st-run-nonane adsorption presents a similar suppression in adsorption as the 1 st-run-water adsorption at the initial P/P_0 range, after which a sharp uprising in adsorption occurs due to pore filling of nonane molecules into micropores. The evident and unclosed desorption hysteresis are characteristic of mesoporosity and that of confinement of nonane molecules in micropores by the enhanced adsorption potential field overlapping from the pore walls of both sides, respectively (Rouquerol et al., 1999). Despite improvement of surface hydrophilicity after the 1 st-run-water adsorption, nonane adsorption in 2 nd-w- and 3 rd-w-runs shows a greater uprising at low P/P_0 range in comparison to that in the 1 st-run adsorption. The smaller nonane adsorption of the 2 nd-w-run in comparison to that of the 1 st-run and of the 3 rd-w-run in comparison to the 2 nd-w-run are, respectively, evidence of loss of one part of porosity after water adsorption and of remaining of one part of micropores in the adsorbent after water adsorption. Thus, the suppressed initial nonane adsorption of the 1 st-run can be ascribed to adsorption of hydrophobic nonane molecules on one part of active sites on the pore surface of $GOC_{16}S$-823 with polarity stronger than the hydroxyl groups which were formed by the 1-st run water adsorption. We suggest that these active sites are groups of defective sites such as $-\text{Si}^{\delta+} \cdots \text{O}^{\delta-}-$ which are formed by decomposition of GO layers and silanol –OH groups during carbonization procedure, and can induce water dissociative adsorption upon water introduction.

As can be observed from the FT-IR spectra shown in the inset of Fig. 1, enhancement in intensity of silanol

–OH groups at around 970 cm^{-1} and a blue shift of the Si—O—Si asymmetric mode (LO mode) around 1200–1300 cm^{-1} (Muroya, 1999) after water adsorption on $GOC_{16}S$-823 supports the consideration that the improved hydrophilicity is owing to the increase in the amount of –OH groups and indicates that the Si-O-Si network structure further develops after water adsorption.

3.2. Nitrogen Adsorption Before and After Nonane and Water Pre-Adsorption

Figure 3 shows the nitrogen adsorption isotherms at 77 K on $GOC_{16}S$-823 before and after nonane pre-adsorption after various treatment steps. The nitrogen adsorption isotherm on $GOC_{16}S$-823 without nonane pre-adsorption presents a composed shape of types I and IV, indicating the co-existence of micropores and mesopores inside the adsorbent (Gregg and Sing, 1982; Sing et al., 1985; Rouquerol et al., 1999). Treatment by step n-1 after nonane pre-adsorption leads to a nitrogen adsorption isotherm with a same shape as that of the 1 st-run but with a smaller adsorption amount due to confinement of nonane molecules in micropores. The differential adsorption isotherm between the two gives an isotherm typical of an excellent type I, characteristic of the inverse imprint of the filled micrpores. The

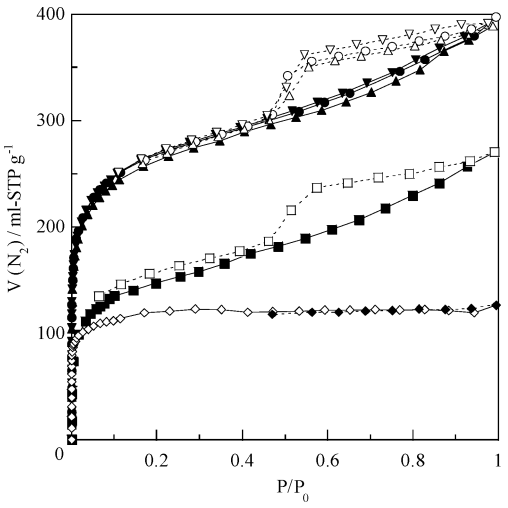

Figure 3. N_2 adsorption isotherms at 77 K on $GOC_{16}S$-823 of the 1 st-run (●, ○) and after steps n-1 (■, □), −2 (▲, △), -3 (▼, ▽) of nonane pre-adsorption, and the differential isotherms between those of the 1 st-run and after step n-1 (⧫, ◇).

pre-adsorbed nonane molecules can be (almost) completely desorbed by evacuation at a temperature above 393 K. This behavior is very similar to that in the case of silica-pillared manganese oxides (Wang et al., 2004) but different from that in the case of carbonaceous materials (Gregg and Sing, 1982), indicating that the micropore surface may be of hyodrophilicity, as discussed in the above section, which is inclined to reject the hydrophobic nonane adsorbate. Because of the composed porosities, the porous parameters of micropore and mesopore cannot be easily separately determined. Here, we estimate the total specific surface areas, S_{BET}, determined from the linearity of Brunauer-Emmett-Teller (BET) plots at the range of $P/P_0 = 0.05$ to 0.1, the total pore volume, $V_{0,0.95}$, calculated from the adsorption value at $P/P_0 = 0.95$, and the lost micropore volume, $V_{mi.loss}$, from the horizontal adsorption in the differential isotherm, and calculate the mesoporous volume, $V_{me,BJH}$, and mesoporous radius, $R_{P,BJH}$, from the Barrett-Joyner-Halenda (BJH) method (Gregg and Sing, 1982; Rouquerol et al., 1999), and the retained micropore volume after each step, $V_{mi,re}$, from the difference of $V_{0,0.95}$ and $V_{me,BJH}$. Table 1 shows the values of porous parameters. About 45% of microporosity can strongly confine nonane molecules inside their pores while almost mesopores and the retained micropores, which should have a larger micropore size, are opened by treatment of step n-1. The slight increase in $V_{me,BJH}$, accompanied by a simultaneous decrease in $V_{mi,re}$ value and increase in $R_{P,BJH}$ value after treatment of step n-3 can be attributed to a little progress in aggregation between small silica particles by another 823 K-evacuation.

Figure 4 shows the nitrogen adsorption isotherms at 77 K on $GOC_{16}S$-823 before and after water pre-adsorption. In contrast to the above nonane pre-adsorption, even treatment by step w-3 (at 823 K) does not lead to the re-opening of all the pores, indicating permanent loss of one part of porosities, in well agreement with the nonane adsorption result of the above section. The Type I-shape differential adsorption isotherm manifests that the lost part of porosity are micropores. However, the lower nitrogen adsorption after treatment of step wn-1 together with the results of the above 2 nd-w- and 3 rd-w-runs nonane adsorption indicate that one part of micropores are still retained after water adsorption. The porous parameters after water pre-adsorption were calculated by the same method as that after nonane-pre-adsorption and shown in Table 1. Result by treatment of step w-1 indicates the loss of

Table 1. Pore parameters of $GOC_{16}S$-823 from N_2 adsorption before and after various pre-adsorption procedures.

Procedure	S_{BET} ($m^2\ g^{-1}$)	$V_{0,total}$ (ml g^{-1})	$V_{me,BJH}$ (ml g^{-1})	$V_{mi,re}$ (ml g^{-1})	$V_{mi,loss}$ (ml g^{-1})	$R_{P,BJH}$ (nm)	D_s
Without pre-adsorption	1010	0.591	0.282	0.309		1.96	
After step n-1	580	0.405	0.267	0.138	0.186	1.96	2.76-mi
After step n-2	985	0.588	0.287	0.301		2.15	
After step n-3	1015	0.596	0.324	0.272		2.05	
After step w-1	565	0.408	0.256	0.152		2.05	
After step w-2	575	0.414	0.259	0.155		2.05	
After step w-3	595	0.429	0.294	0.135	0.162	2.05	2.79-mi
After step wn-1	265	0.281	0.246	0.035	0.148	2.05	2.88-mi
							2.45-me

about 49% of microporosites, whose ratio is very close to that lost by nonane pre-adsorption after step n-1. Again another 823 K-evacuation (step w-3) after water adsorption induces further aggregation of silica particles, resulting in a corresponding increase in $V_{me,BJH}$, and decrease in $V_{mi,re}$. The near-zero-$V_{mi,re}$ value after treatment of step wn-1 indicates that all the retained micropores after water pre-adsorption have a size enough small to sufficiently confine nonane molecules. Furthermore, an unexpected larger $V_{mi,loss}$ value after step wn-1 is attributed to the loss of little part of mesopores which indicates existence of one part of ink-bottle-type pore structure with a neck of micropore size.

In our previous report (Wang et al., 2003), porosities of another $GOC_{16}S$-823 sample have been analyzed in detail by high-resolution α_s-plot and the result on porosity change upon high temperature calcination suggests that microporosities and mesoporosities of the adsorbent are constructed of aggregates of small silica particles and the interstitial space between carbon layers and silica particles, respectively. The above pre-adsorption results, especially, the loss of microporosities due to water adsorption, strongly support this conclusion. Since the aggregates of (round) silica particles give a three dimensional pore surface and pore surface involving carbon layers should have a more two dimensional geometry, separated fractal analysis on the adsorption data of the inverse imprint of microporosity and the retained mesoporosity after nonane or water pre-adsorption can provide more evidence for the above consideration. The surface fractal constancy, D_s, regarding pore surface geometry can be obtained from analysis of the following Frenkel-Halsey-Hill equation using a single probe adsorbate (Pfeifer et al., 1989):

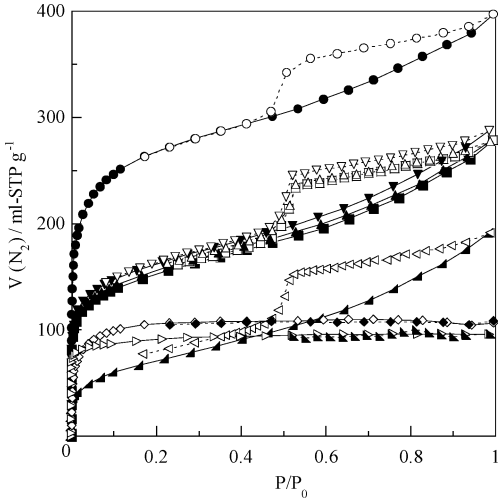

Figure 4. N_2 adsorption isotherms at 77 K on $GOC_{16}S$-823 of the 1 st-run (●, ○) and after steps w-1 (■, □), -2 (▲, △), -3 (▼, ▽), wn-1 (◢, ◁) of H_2O pre-adsorption, and the differential isotherms between those of the 1 st-run and after step w-3 (◇, ♦) and between those after step w-3 and after wn-1 (▷, ◣).

$$V = B[\ln(P_0/P)]^{Ds-3} \quad (1)$$

where P and P_0 are the pressure and saturated pressure, V the adsorption amount, and B the constant. Avnir et al. (Janoniec et al., 1990) derived a same equation from Dubinin-Stoeckli relation (Gregg and Sing, 1982) for analysis of micropore surface. Fractal analysis were carried out for the differential isotherms between nitrogen adsorption isotherm of the 1 st-run and that after each of steps n-1 and w-3, and between those after steps w-3 and wn-1, which only have microporosity, and for

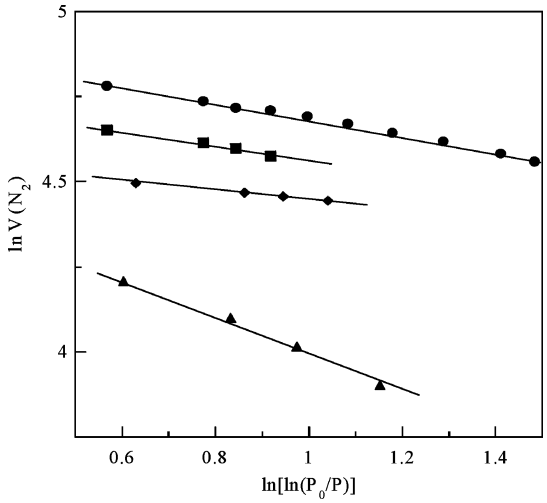

Figure 5. The ln $V(N_2)$ vs ln[ln(P_0/P)] plots for the differential N_2 adsorption isotherms of the 1 st-run and that after step n-1 (●), of the 1 st-run and that after step w-3 (■), and of those after steps w-3 and wn-1 (♦), and for the N_2 adsorption isotherm after step wn-1 (▲).

the nitrogen adsorption isotherm after step wn-1, which almost has only mesoporosity. Figure 5 shows the relationship of ln $V(N_2)$ and ln[ln(P_0/P)] obtained from Eq. (1). All the plots show a linearity at $P/P_0 = 0.01$ to 0.15. A higher slope for the plot of nitrogen adsorption isotherm after step wn-1 in comparison to the others indicates that the mesopore surface has a less roughness than the micropore surface. The D_s values were calculated from the slope of these plots and shown in Table 1 (placed at the same line of the corresponding pre-adsorption treatment step with a tailing mark of –mi or –me denoting micropore or mesopore). All the D_s values of micropore surface are greater than 2.76 while that of mesopore surface ($D_s = 2.45$) are closer to that of a two-dimensional surface ($D_s = 2$). Thus, fractal analysis supports the consideration that micropores with rougher surface geometry in the composite are surrounded by small silica particles, which are partly lost by H_2O introduction, and mesopores with flatter surface geometry involve the carbon layers.

4. Conclusion

A novel nanoporous C/SiO_2 composite was synthesized using graphite as the precursor by a soft chemical method and its adsorption properties were characterized by nonane, water, and nitrogen adsorption. Only one part of micropores can strongly confine nonane molecules, indicating a wide micropore size distribution. While leaving one part of micropores with smaller pore width and retaining the most part of mesopores, water adsorption leads to disappearance of one part of micropores. Loss of micropores upon water adsorption is attributed to the closing of micropores by dissociated adsorption of water on defective sites in $GOC_{16}S$-823, which improves the surface hydrophilicity by forming hydroxyl groups and Si—O—Si networking. Fractal analysis of the original or the differential nitrogen adsorption isotherms indicates that micropore surface has a rougher geometry with $D_s > 2.76$ and mesopore surface has a flatter geometry with $D_s = 2.45$, suggesting that micropores are constructed of small silica particles and mesopores involve the flat carbon layers.

References

Barrer, R.M., *Zeolites and Clay Minerals as Sorbents and Molecular Sieves*, Academic Press, New York, 1978.

Barton, T.J., L.M. Bull, W.G. Klemperer, D.A. Loy, B. McEnaney, M. Misono, P.A. Monson, G. Pez, G.W. Scherer, J.C. Vartuli, and O.M. Yaghi, *Chem. Mater.*, **11**, 2633 (1999).

Dresselhaus M.S. and K.A. William, *MRS Bull.*, **24**, 45 (1999).

Gregg, S.J. and K.S.W. Sing, *Adsorption, Surface Area, and Porosity*, Academic, New York, 1982.

Inagaki, S., Y. Fukushima, and K. Kuroda, *J. Chem. Soc. Chem. Comm.*, 680 (1993).

Janoniec, M., X. Lu, R. Maday, and D. Avnir, *J. Chem. Phys.*, **92**, 7589 (1990).

Landi, M.E., B.A. Aufdembrink, P. Chu, I.D. Jonhson, G.W. Kirker, and M.K. Rubin, *J. Am. Chem. Soc.*, **113**, 3189 (1991).

Marsh, H., *Introduction to Carbon Science*, Butterworths, London, 1989.

Matranga, K.R., A.L. Myers, and E.D. Glandt, *Chem. Eng.*, **7**, 1569 (1992).

Muroya, M., *Colloid and Surfaces*, **157**, 147–155 (1999).

Pfeifer, P., Y.J. Wu, M.W. Cole, and J. Krim, *Phys. Rev. Lett.*, **62**, 1997 (1989).

Pinnavaia, T.J., *Science*, **220**, 365 (1983).

Radovic, L.R. and F. Rodriguez-Reinoso, *Chem. Phys. Carbon*, **25**, 243 (1997).

Rouquerol, F., J. Rouquerol, and K.S.W. Sing, *Adsorption by Powders & Porous Solids*, Academic, San Diego, 1999.

Sing, K.S.W., D.H. Everett, R.A.W. Haul, L. Moscou, R.A. Pierotti, J. Rouquerol, and T. Siemieniewska, *Pure Appl. Chem.*, **57**, 603 (1985).

Staudenmaier, L., *Ber Deutsche Chem. Ges.*, **31**, 1481 (1898).

Wang, Z.-M., K. Hoshinoo, K. Shishibori, H. Kanoh, and K. Ooi, *Chem. Mater.*, **15**, 2926 (2003).

Wang, Z.-M., K. Hoshinoo, M. Xue, H. Kanoh, and K. Ooi, *Chem. Commun.*, 1696 (2002).

Wang, Z.-M., N. Yamashita, and H. Kanoh, *J. Colloid and Interface Science*, **269**, 283 (2004).

Yamanaka, S. and G.W. Brindly, *Clays Clay Miner.*, **26**, 21 (1978).

Yanagisawa, T., T. Shimizu, K. Kuroda, and C. Kato, *Bull. Chem. Soc. Jpn.*, **63**, 988 (1990).